

Finite Temperature Effects in Ultracold Fermi Gases

K. LEVIN and QIJIN CHEN

James Franck Institute and Department of Physics, University of Chicago, Chicago, Illinois 60637, USA

1. – BCS-BEC Crossover Theory and the Physical Effects of Temperature

The study of ultracold trapped fermionic gases is a rapidly exploding subject [1-10] which is defining new directions in condensed matter and atomic physics. It has also captured the attention of physicists who study color superconducting quark matter as well as nuclear matter [11-13]. Indeed, it is hard, in recent times, to find a subfield of physics which appeals this broadly to the research community. As we come to understand the gases, experimentalists will move to address fermionic atoms in optical lattices; this will provide important insight to condensed matter physicists as analogue systems for “solving” intractable many body problems.

What makes these gases (and lattices) so important is their remarkable tunability and controllability. Using a Feshbach resonance, one can tune the attractive two-body interaction from weak to strong, and thereby make a smooth crossover from a BCS superfluid to a Bose-Einstein condensation (BEC) [14, 15]. Not only does this allow high transition temperatures T_c (relative to the Fermi energy E_F) but it may also provide insights into the high temperature cuprate superconductivity [16-19]. Furthermore, one can tune the population of the two spin states, essentially at will, in this way, allowing exploration [20-22] of exotic polarized phases such as the FFLO [23-25] superfluids, of interest to condensed matter, nuclear and particle physicists. One will be able to tune the lattice parameters such as bandwidth, on-site repulsion, even random disorder, etc and thereby study the famous, and as yet, unsolved Hubbard model Hamiltonian.

This paper will concentrate on those issues relating to the effects which are of current interest to experimentalists. In particular, we will study BCS-BEC crossover in atomic Fermi gases, looking at a wide range of different experiments. Our group has been principally interested in the effects of finite temperature [26, 17, 18] and in this review, we will discuss how temperature T enters into the standard crossover theory, and how temperature can be measured, and how tem-

perature changes the character of the gas from a superfluid at low T to an unusual (but strongly interacting) normal fluid at moderate T , and to ultimately a Fermi gas at high T . Temperature, of course, plays an important role in these Fermi gas experiments. As we shall see in this Review, the earliest evidence for superfluidity is generally based [1-8] on a comparison of the behavior of the gas at two different temperatures, presumably, one above and one below T_c . Experimentally, one is never strictly at $T = 0$, and as a result there are thermal excitations of the gas which need to be characterized both theoretically and experimentally.

Before we begin with the ultracold gases, it is useful to discuss to what extent the BCS-BEC crossover scenario relates to the high temperature copper oxide superconductors [17, 18]. While there is much controversy in the field of high T_c superconductivity, there is a school of thought [17, 27-31, 19] which argues that these systems are somewhere intermediate between BCS and BEC. These arguments are based on the observation that T_c is anomalously high, and therefore the attractive interaction is presumably stronger than in conventional superconductors. These are quasi-two-dimensional (2D) materials which means that they have a tendency to exhibit “pre-formed” pairs, that is, pairing in advance of Bose condensation. This is often referred to as fluctuation effects, but pre-formed pairs are naturally associated with a more BEC-like scenario. Importantly these pairs can be used to explain the widespread and anomalous “pseudogap” effects [16, 32] which are the focus [33] of most of the current attention in the field. The existence of “pre-formed” pairs means that a characteristic (pseudogap) energy must be supplied in the normal state to break the pairs and create fermionic excitations. Hence we say that there is a gap or, more precisely, a pseudogap in the fermionic excitation spectrum.

The case that the crossover scenario is relevant to the cuprates was made quite eloquently by A. J. Leggett in a recent status report [19] on high T_c superconductivity. In this article he summarized the eight salient “facts” about the cuprates. It is worth quoting one here, which relates to their anomalously short coherence length. *“The size of the pairs is somewhere in the range 10-30 Å – from measurements of the upper critical field, Fermi velocity and T_c . This means that the pair size is only moderately greater than the inter-conduction electron in-plane spacing, putting us in the intermediate regime of the so-called Bose-Einstein condensate to BCS superconductor (BEC-BCS) crossover, and leading us to expect very large effects of fluctuations (they are indeed found).”*

The field of BCS-BEC crossover is built around early observations by Eagles [15] and Leggett [14] that the BCS ground state, proposed by Bardeen, Cooper, and Schrieffer in 1957, is much more general than was originally thought. If one increases the strength of the attraction and self-consistently solves for the fermionic chemical potential μ , this wave function will correspond to a more BEC-like form of superfluidity. Knowing the ground state what is the nature of the superfluidity at finite T ? That is the central question we will address in this Review.

Even without a detailed theoretical framework we can make three important observations.

- As we go from BCS to BEC, pairs will form above T_c without condensation. In the normal state, it pays in general to take advantage of the attractive pairing interaction. Only in the extreme BCS limit do pairs form exactly at T_c .
- The fundamental statistical entities in these superfluids are fermions. We can think of pairs of fermions as a form of “boson”, although the statistics are not precisely the same.

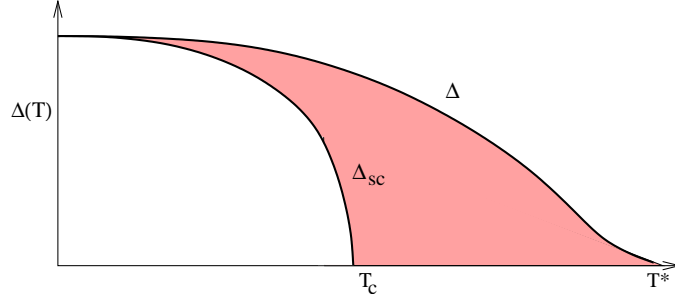


Figure 1. – Contrasting behavior of the excitation gap $\Delta(T)$ and superfluid order parameter $\Delta_{sc}(T)$ versus temperature. The height of the shaded region roughly reflects the density of noncondensed pairs at each temperature.

We measure these “bosonic” or pair-degrees of freedom indirectly via the fermionic gap parameter $\Delta(T)$. In the fermionic regime this parameter is the minimum energy which must be supplied to create fermionic excitations. It tells us about bosons indirectly through the binding together of two fermions.

- In general there will be two types of excitations in these BCS-BEC crossover systems. Only in strict BCS theory are the excitations of solely fermionic character, and only in the strict BEC limit will the excitations be solely of bosonic character. More generally in the intermediate case (often called the “unitary” regime) the excitations consist of a mix of both fermions and bosons.

These observations are illustrated by Figs. 1 and 2. In Fig. 1 we schematically plot the gap parameter $\Delta(T)$ as a function of T , along with the superfluid order parameter $\Delta_{sc}(T)$. The former, which represents the “bosonic” degrees of freedom, shows that pairs continuously form once temperature is less than a crossover temperature T^* , while the order parameter turns on as in a second order phase transition at T_c . The height of the shaded region reflects the number of noncondensed pairs. This number increases monotonically with decreasing T , until T_c is reached. A T further decreases below T_c the number of noncondensed pairs begins to decrease monotonically due to the condensation of zero momentum pairs.

In Fig. 2 we present a schematic plot of the excitation type, which shows that between BCS and BEC (i.e., in the unitary regime) there will be a mix of fermions and bosons. These bosons and fermions are not separate fluids, but rather they are strongly inter-connected. Indeed, the gap in the fermionic spectrum (related to Δ) is a measure of the number of bosons in the system.

2. – Theory Outline

In this paper we will presume the ground state is given by the standard BCS-like wavefunction,

$$(2.1) \quad \Psi_0 = \prod_{\mathbf{k}} (u_{\mathbf{k}} + v_{\mathbf{k}} c_{\mathbf{k},\uparrow}^\dagger c_{-\mathbf{k},\downarrow}^\dagger) |0\rangle,$$

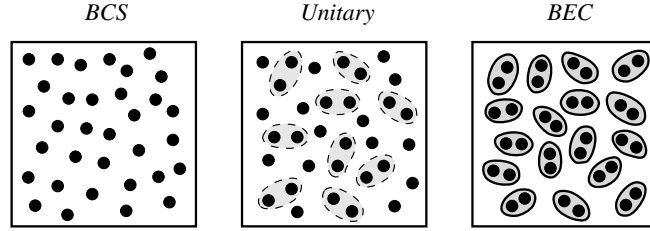


Figure 2. – Schematic illustration of excitations in the BCS, unitary and BEC regimes. The black discs represent fermionic excitations. Pair excitations become progressively dominant as the system evolves from the BCS to BEC regime.

where $c_{\mathbf{k},\sigma}^\dagger$ and $c_{\mathbf{k},\sigma}$ are the creation and annihilation operators for fermions of momentum \mathbf{k} and spin $\sigma = \uparrow, \downarrow$. The variational parameters $v_{\mathbf{k}}$ and $u_{\mathbf{k}}$ are usually represented by the two more directly accessible parameters $\Delta_{sc}(T = 0)$ and μ , which characterize the fermionic system. Here $\Delta_{sc}(T = 0)$ is the zero temperature superconducting order parameter. These fermionic parameters are uniquely determined in terms of the attractive interaction U and the fermionic density n . The variationally determined self consistency conditions are given by two BCS-like equations which we refer to as the “gap” and “number” equations, respectively.

At $T = 0$, the effects of BEC-BCS crossover are most directly reflected in the behavior of the fermionic chemical potential μ , which is associated with the number equation. We plot the behavior of μ in Fig. 3, which indicates the BCS and BEC regimes. In the weak coupling regime $\mu = E_F$ and ordinary BCS theory results. With increasing $|U|$, μ begins to decrease, eventually crossing zero and then ultimately becoming negative in the BEC regime. We generally view

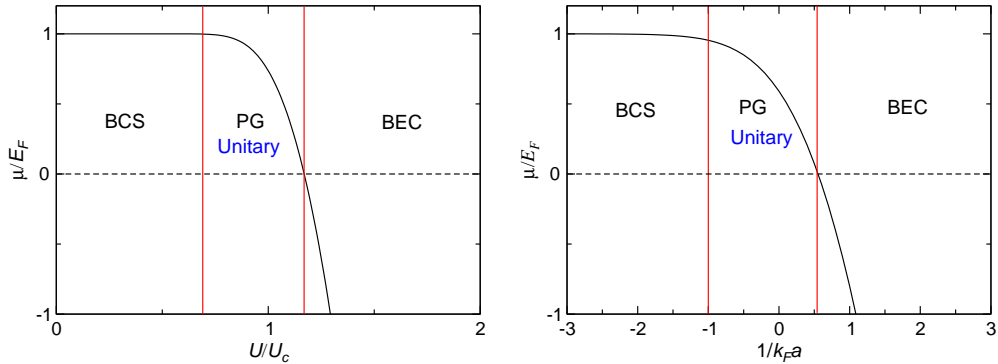


Figure 3. – Typical behavior of the chemical potential μ at $T = 0$ in the three regimes, as a function of the interaction strength U/U_c , or, equivalently, $1/k_F a$. As U/U_c increases from 0, the chemical potential μ starts to decrease and then becomes negative. The character of the system changes from fermionic ($\mu > 0$) to bosonic ($\mu < 0$). The pseudogap (PG) or unitary regime corresponds to non-Fermi liquid based superconductivity, and $U_c (< 0)$ corresponds to critical coupling for forming a two fermion bound state in vacuum [17], i.e., the unitary point where the two-body s -wave scattering length a diverges.

TABLE I. – BCS theory by way of BEC analogy. Here we compare condensation in composite and point bosons; μ_B is the bosonic chemical potential, N_0 and N_T are the number of condensed and noncondensed bosons, respectively. We define μ_{pair} as the chemical potential for the noncondensed pairs. Here $\Delta(T)$ is the total fermionic gap which contains contributions from the noncondensed (Δ_{pg}^2) and condensed terms (Δ_{sc}^2). In the strict BCS limit $\Delta_{pg} = 0$, so that the order parameter and gap are identical.

	Composite bosons	Point bosons
Pair chemical potential	$\mu_{pair} = 0, T \leq T_c$ Leads to BCS gap equation for $\Delta(T)$	$\mu_B = 0, T \leq T_c$
Total “number” of pairs	$\Delta^2(T) = \Delta_{sc}^2(T) + \Delta_{pg}^2(T)$	$N = N_0 + N_T$
Noncondensed pairs	$Z\Delta_{pg}^2 = \sum_{\mathbf{q} \neq 0} b(\Omega_{\mathbf{q}})$	$N_T = \sum_{\mathbf{q} \neq 0} b(\Omega_{\mathbf{q}})$

$\mu = 0$ as a crossing point. For positive μ the system has a remnant of a Fermi surface, and we say that it is “fermionic”. For negative μ , the Fermi surface is gone and the material is “bosonic”.

One can debate whether other ground states ought to be considered. Indeed the work of the Camerino group [34, 35] is based on a finite T approach first introduced by Nozieres and Schmitt-Rink (NSR) [36, 31]. This leads to a different, and not as readily characterized ground state. We list some arguments in support of the ground state in Eq. (2.1). (i) This is the basis for the widely studied Bogoliubov-de Gennes approach, which can be applied [37-40] to the BCS-BEC crossover problem at $T = 0$. (ii) At arbitrarily strong coupling (and $T = 0$), this ground state can be shown to coincide with a Gross-Pitaevskii (GP) description [41] of the boson system. (iii) This ground state is the basis for the rapidly proliferating theoretical literature [40, 42-47] on spin polarized Fermi superfluids. In addition to our own work there have been some additional studies which include the effects of temperature [48-50], albeit at a lower order mean field theory than considered here.

We begin at the more physical level by stressing the analogy between condensation in this composite boson or fermionic superfluid and condensation in a gas of ideal point bosons. Our microscopic theory treats self-consistently two-particle and one-particle Green’s functions on an equal footing. Because the physics is so simple and clear, we can fairly readily anticipate the form of the central equations of this BCS-BEC generalization of BCS theory. It is important to stress, however, that these equations can be derived more rigorously from a truncated series of equations of motion for the appropriate Green’s functions [16, 51].

There are three principal equations which govern Bose condensation: the vanishing of the bosonic chemical potential at all $T \leq T_c$ is the first. We will refer to this condition as the “BEC condition”. It is related to the usual Thouless criterion for superconductivity, but the latter is generally associated only with the temperature T_c . The second equation is the boson number equation. All “bosons” must be accounted for as either condensed or noncondensed. The third equation is the number of noncondensed “bosons”, which are created by thermal excitations. This is determined simply by inserting the known excitation spectrum of the excited pairs or bosons, into the Bose distribution function $b(x)$. With this equation, and the second equation,

one can then deduce the number of condensed bosons.

These three central equations for bosons are indicated in Table I, on the far right, for true point bosons, and in the second column for the composite bosons which appear in fermionic superfluids. For these composite bosons the quantity which provides a measure of the “number” of bosons (N) is given by $\Delta^2(T)$ (up to a constant coefficient, Z). How does one quantitatively establish the appropriate “boson number” for the fermionic case? This is determined via the self consistent gap equation for $\Delta(T)$, which, in turn, is determined using the first condition: that the pair chemical potential μ_{pair} is zero at and below T_c . How does one compute the number of excited pairs? Once the gap equation is interpreted in terms of the appropriate noncondensed pair propagator (see below), then one knows the related excitation spectrum Ω_q of this propagator.

The quantity Z which appears in the last equation of the Table (for the composite bosons) gives the relation between the gap associated with noncondensed pairs (Δ_{pg}^2) and the number of all pairs [$\sum b(\Omega_q)$]. It can be readily calculated in this theory; once one has the noncondensed pair propagator, Z appears as the inverse residue. (Deep in the BEC regime [52], Z is relatively simple to compute, for here the boson number density approaches the asymptote $n/2$). More precisely, the total number of bosons in the present case has to be determined self-consistently through the gap equation for $\Delta(T)$. It also involves the fermion number equation through the related fermionic chemical potential.

To be consistent with the ground state variational conditions, the vanishing of the pair chemical potential is associated with a particular form for the pair propagator involving dressed Green’s functions. These, in turn, determine the fermionic chemical potential through the fermion number equation.

2.1. Microscopic T -matrix Scheme. – Next, we implement this picture microscopically via a T -matrix approximation. We include spin indices throughout so that it will be clear how to apply this scheme to spin polarized superfluids. This means that we consider the coupled equations between the particles (with propagator G) and the pairs [with propagator $t(P)$] and drop all higher order terms. This theory does not include direct “boson-boson” interactions, although the pairs do interact indirectly via the fermions, in an averaged or mean field sense. Here, for all $T \leq T_c$, the BEC condition is interpreted as requiring that the pair chemical potential μ_{pair} associated with the noncondensed pairs, vanish. Within a T -matrix scheme, the pair propagator is given by

$$(2.2) \quad t_{pg}^{-1}(P) = U^{-1} + \chi(P),$$

where χ is the pair susceptibility. The function $\chi(P)$ is, in many ways, the most fundamental quantity we introduce. We will show that one obtains consistent answers between T -matrix based approaches and the BCS-Leggett ground state equations, provided the components of the pair susceptibility, defined by

$$(2.3) \quad \chi(P) = \frac{1}{2} [\chi_{\uparrow\downarrow}(P) + \chi_{\downarrow\uparrow}(P)]$$

are given by the product of one dressed and one bare Green's function

$$(2.4) \quad \chi_{\uparrow\downarrow}(P) = \sum_K G_{0\uparrow}(P-K)G_{\downarrow}(K), \quad \chi_{\downarrow\uparrow}(P) = \sum_K G_{0\downarrow}(P-K)G_{\uparrow}(K),$$

where $P = (i\Omega_l, \mathbf{p})$, and G and G_0 are the full and bare Green's functions respectively. Here $G_{0,\sigma}^{-1}(K) = i\omega_n - \xi_{\mathbf{k},\sigma}$, $\xi_{\mathbf{k},\sigma} = \epsilon_{\mathbf{k}} - \mu_{\sigma}$, $\epsilon_{\mathbf{k}} = \hbar^2 k^2/2m$ is the kinetic energy of fermions, and μ_{σ} is the fermionic chemical potential for spin $\sigma = \uparrow, \downarrow$. Throughout this paper, we take $\hbar = 1$, $k_B = 1$, and use the four-vector notation $K \equiv (i\omega_n, \mathbf{k})$, $P \equiv (i\Omega_l, \mathbf{q})$, $\sum_K \equiv T \sum_n \sum_{\mathbf{k}}$, etc, where $\omega_n = (2n+1)\pi T$ and $\Omega_l = 2l\pi T$ are the standard odd and even Matsubara frequencies [53] (where n and l are integers).

We now evaluate the BEC condition

$$(2.5) \quad t_{pg}^{-1}(0) = 0 = U^{-1} + \chi(0).$$

The one-particle Green's function for fermions with spin σ is

$$(2.6) \quad G_{\sigma}^{-1}(K) = G_{0\sigma}^{-1}(K) - \Sigma_{\sigma}(K) = i\omega_n - \xi_{k\sigma} - \Sigma_{\sigma}(K),$$

where $\bar{\sigma} \equiv -\sigma$, and the self-energy Σ_{σ} is of the BCS-like form

$$(2.7) \quad \Sigma_{\sigma}(K) = -\Delta^2 G_{0\bar{\sigma}}(-K) = \frac{\Delta^2}{i\omega + \xi_{k\bar{\sigma}}}.$$

It should be noted that we use a contact potential so that the symmetry factor $\varphi_{\mathbf{k}}$ associated with the pairing interaction is trivially $\varphi_{\mathbf{k}} = 1$. For a nontrivial $\varphi_{\mathbf{k}}$, one only needs to replace Δ with $\Delta\varphi_{\mathbf{k}}$ in Eq. (2.7). We will see below how this form for the self energy very naturally arises (below T_c) in a T -matrix approach. Thus

$$(2.8) \quad G_{\sigma}^{-1}(K) = i\omega - \xi_{k\sigma} - \frac{\Delta^2}{i\omega + \xi_{k\bar{\sigma}}}.$$

Now we are in position to calculate the pair susceptibility at $P = 0$

$$(2.9) \quad \chi(0) = \chi_{\uparrow\downarrow}(0) = \chi_{\downarrow\uparrow}(0) = - \sum_K \frac{1}{(i\omega_n - E_{k\downarrow})(i\omega_n + E_{k\uparrow})}.$$

Substituting this expression into our BEC condition Eq. (2.5), we obtain the gap equation

$$(2.10) \quad 0 = \frac{1}{U} + \sum_{\mathbf{k}} \left[\frac{1 - f(E_{k\downarrow}) - f(E_{k\uparrow})}{2E_k} \right] = \frac{1}{U} + \sum_{\mathbf{k}} \frac{1 - 2\bar{f}(E_k)}{2E_k}.$$

after carrying out the Matsubara summation. Here $\mu = (\mu_{\uparrow} + \mu_{\downarrow})/2$ and $h = (\mu_{\uparrow} - \mu_{\downarrow})/2$, $E_{\mathbf{k}} = \sqrt{\xi_{\mathbf{k}}^2 + \Delta^2}$, $E_{k\uparrow} = -h + E_k$ and $E_{k\downarrow} = h + E_k$, where $\xi_{\mathbf{k}} = \epsilon_{\mathbf{k}} - \mu$. In addition,

we define the average $\bar{f}(x) \equiv [f(x+h) + f(x-h)]/2$, where $f(x)$ is the Fermi distribution function.

The coupling constant U can be replaced in favor of the dimensionless parameter, $1/k_F a$, via the relationship $m/(4\pi a) = 1/U + \sum_{\mathbf{k}} (2\epsilon_{\mathbf{k}})^{-1}$, where a is the two-body s -wave scattering length, and k_F is the noninteracting Fermi wave vector for the same total number density in the absence of population imbalance. Therefore the gap equation can be rewritten as

$$(2.11) \quad -\frac{m}{4\pi a} = \sum_{\mathbf{k}} \left[\frac{1 - 2\bar{f}(E_{\mathbf{k}})}{2E_{\mathbf{k}}} - \frac{1}{2\epsilon_{\mathbf{k}}} \right].$$

Here the ‘‘unitary scattering’’ limit corresponds to resonant scattering where $a \rightarrow \infty$. This scattering length is tunable by magnetic field application and we say that we are on the BCS or BEC side of resonance, depending on whether the fields are higher or lower than the resonant field, or alternatively whether a is negative or positive, respectively.

Finally, in terms of Green’s functions, we readily arrive at the number equations: $n_{\sigma} = \sum_K G_{\sigma}(K)$, which are consistent with their ground state counterparts

$$(2.12) \quad n_{\sigma} = \sum_{\mathbf{k}} [f(E_{\mathbf{k}\sigma})u_{\mathbf{k}}^2 + f(E_{\mathbf{k}\bar{\sigma}})v_{\mathbf{k}}^2],$$

where the coherence factors $u_{\mathbf{k}}^2, v_{\mathbf{k}}^2 = (1 \pm \xi_{\mathbf{k}}/E_{\mathbf{k}})/2$.

Next we use this T -matrix scheme to derive Eq. (2.7) and separate the contribution from condensed and noncondensed pairs. The diagrammatic representation of our T -matrix scheme is shown in Fig. 4. The first line indicates t_{pg} , and the second the total self energy. One can see throughout the combination of one dressed and one bare Green’s function, as represented by the thick and thin lines. The self energy consists of two contributions from the noncondensed pairs or pseudogap (pg) and from the condensate (sc). There are, analogously, two contributions in the full T -matrix

$$(2.13) \quad t = t_{pg} + t_{sc},$$

$$(2.14) \quad t_{pg}(P) = \frac{U}{1 + U\chi(P)}, \quad P \neq 0,$$

$$(2.15) \quad t_{sc}(P) = -\frac{\Delta_{sc}^2}{T}\delta(P),$$

where we write $\Delta_{sc} = -U \sum_{\mathbf{k}} \langle c_{-\mathbf{k}\downarrow} c_{\mathbf{k}\uparrow} \rangle$.

Similarly, we have for the fermion self energy

$$(2.16) \quad \Sigma_{\sigma}(K) = \Sigma_{\sigma}^{sc}(K) + \Sigma_{\sigma}^{pg}(K) = \sum_P t(P)G_{0,\bar{\sigma}}(P-K).$$

We can see at once that

$$(2.17) \quad \Sigma_{\sigma}^{sc}(K) = \sum_P t_{sc}(P)G_{0,\bar{\sigma}}(P-K) = -G_{0,\bar{\sigma}}(-K)\Delta_{sc}^2.$$

The vanishing of the pair chemical potential implies that

$$(2.18) \quad t_{pg}^{-1}(0) = U^{-1} + \chi(0) = 0, \quad T \leq T_c.$$

Moreover, a vanishing chemical potential means that $t_{pg}(P)$ diverges $P = 0$. Thus, we may approximate [54] Eq. (2.16) to yield

$$(2.19) \quad \Sigma_\sigma(K) \approx -G_{0,\bar{\sigma}}(-K)\Delta^2,$$

where

$$(2.20) \quad \Delta^2(T) \equiv \Delta_{sc}^2(T) + \Delta_{pg}^2(T),$$

Importantly, we are led to identify the quantity Δ_{pg}

$$(2.21) \quad \Delta_{pg}^2 \equiv - \sum_{P \neq 0} t_{pg}(P).$$

Note that in the normal state (where μ_{pair} is non-zero) Eq. (2.19) is no longer a good approximation.

We now have a closed set of equations for addressing the ordered phase. This approach can be readily generalized [55] to treat more exotic polarized phases such as the LOFF state [23,25,24]. We can similarly extend this approach to temperatures somewhat above T_c , by self consistently including a non-zero pair chemical potential. This is a necessary step in addressing a trap as well [56]. Additionally, the propagator for noncondensed pairs can now be quantified, using the self consistently determined pair susceptibility. At small four-vector P , we may expand the inverse of t_{pg} , after analytical continuation ($i\Omega_l \rightarrow \Omega + i0^+$), to obtain

$$(2.22) \quad t_{pg}^{-1} \approx a_1\Omega^2 + Z \left(\Omega - \frac{p^2}{2M^*} + \mu_{pair} + i\Gamma_P \right),$$

where the imaginary part $\Gamma_P \rightarrow 0$ rapidly as $p \rightarrow 0$ below T_c . Because we are interested in the moderate and strong coupling cases, we drop the $a_1\Omega^2$ term in Eq. (2.22), and hence

$$(2.23) \quad t_{pg}(P) = \frac{Z^{-1}}{\Omega - \Omega_p + \mu_{pair} + i\Gamma_P},$$

where we associate

$$(2.24) \quad \Omega_p \approx \frac{p^2}{2M^*}.$$

This establishes a quadratic pair dispersion and defines the effective pair mass, M^* . They can be calculated via a small p expansion of $\chi(P)$,

$$(2.25) \quad Z = \left. \frac{\partial \chi}{\partial \Omega} \right|_{\Omega=0, \mathbf{p}=0}, \quad \frac{1}{2M^*} = - \left. \frac{1}{6Z} \frac{\partial^2 \chi}{\partial p^2} \right|_{\Omega=0, \mathbf{p}=0}.$$

$$t_{pg} = | + \boxed{} + \boxed{} + \boxed{} + \dots$$

$$\Sigma = \text{Diagram 1} + \text{Diagram 2}$$

Figure 4. – T -matrix and self-energy diagrams for the present T -matrix scheme. The self-energy comes from contributions of both condensed (Σ_{sc}) and noncondensed (Σ_{pg}) pairs. Note that there is one dressed and full Green’s function in the T -matrix. Here t_{pg} represents the propagator for the noncondensed pairs.

Finally, one can rewrite Eq. (2.21) as

$$(2.26) \quad \Delta_{pg}^2(T) = Z^{-1} \sum_{\mathbf{p}} b(\Omega_{\mathbf{p}}).$$

We now return to the strong analogies between our T -matrix approach and Bose condensation of point bosons, as summarized in Table I. We have three central equations.

1. The pair chemical potential must vanish at and below T_c ,

$$(2.27) \quad \mu_{pair} = 0, \quad (T \leq T_c).$$

Importantly this condition leads to the mean field gap equation derived in Eq. (2.10).

2. There must be a conservation of the total number of (composite) “bosons” in the system. For this condition, our central equation is Eq. (2.20). Here it is understood that the number of “bosons” is effectively represented by the parameter $\Delta^2(T)$. Unlike the point boson case, the “total boson number” is temperature dependent and has to be self-consistently determined.

3. The number of noncondensed pairs is readily computed in terms of the pair dispersion, just as in conventional BEC. For this condition our central equation is Eq. (2.26). Then, just as in conventional BEC, the number of condensed bosons (proportional to Δ_{sc}^2) is determined by the difference between $\Delta^2(T)$ and $\Delta_{pg}^2(T)$. This, in turn, determines T_c as the lowest temperature(s) in the normal state at which noncondensed pairs exhaust the total weight of Δ^2 so that $\Delta_{pg}^2 = \Delta^2$. Solving for the “transition temperature” in the absence of pseudogap effects [48-50] leads to the quantity T_c^{MF} . More precisely, T_c^{MF} should be thought of as the temperature at which the excitation gap $\Delta(T)$ vanishes. This provides a reasonable estimate, for the pairing onset temperature T^* , (when a stable superfluid phase exists). This is distinguished from the transition temperature. We note that T^* represents a smooth crossover rather than an abrupt phase transition.

It should be stressed that the dispersion relation for the noncondensed pairs is quadratic. While *one will always find a linear dispersion in the collective mode spectrum* [57], within the present class of BCS-BEC crossover theories, the restriction to a T -matrix scheme means that there is no feedback from the collective modes onto the pair excitation spectrum. In effect, the T -matrix approximation does not incorporate pair-pair interactions at a level needed to arrive

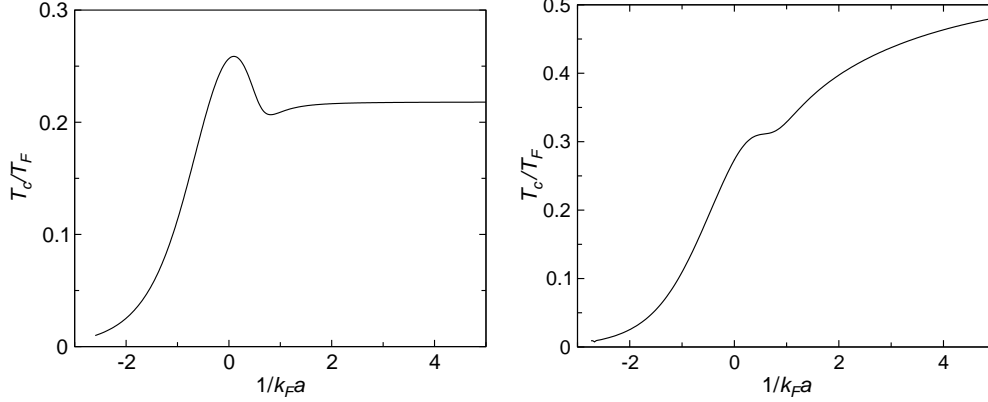


Figure 5. – Typical behavior of T_c as a function of $1/k_F a$ in a homogeneous system (left panel) and in a trapped Fermi gas (right panel). T_c follows the BCS predictions and approaches the BEC asymptote $0.218T_F$ and $0.518T_F$ in the homogeneous and trapped cases, respectively. In contrast to the homogeneous case, the BEC asymptote in a trap is much higher due to a compressed profile for trapped bosons. In the homogeneous case, T_c reaches a maximum around $1/k_F a = 0$ and a minimum around where $\mu = 0$. In the trapped case, this maximum/minimum behavior is washed out largely by the shrinking cloud size as $1/k_F a$ increases.

at this expected linear dispersion in the pair excitation spectrum. Nevertheless, this level of approximation is consistent with the underlying ground state wavefunction.

3. – Behavior of T_c and Trap Effects

Before turning to experiment, it is important to discuss the behavior of T_c which is plotted as a function of scattering length in the left panel of Fig. 5 for the homogeneous case, presuming s -wave pairing. Starting from the BCS regime this figure shows that T_c initially increases as the interaction strength increases. However, this increase competes with the opening of a pseudogap or excitation gap $\Delta(T_c)$. Technically, the pairs become effectively heavier before they form true bound states. Eventually T_c reaches a maximum (very near unitarity) and then decreases slightly until field strengths corresponding to the point where μ becomes zero. At this field value (essentially where T_c is minimum), the system becomes a “bosonic” superfluid, and beyond this point T_c increases slightly to reach the asymptote $0.218E_F$ corresponding to an ideal Bose gas.

Trap effects change these results only quantitatively as seen in the right panel of Fig. 5. Here the maximum in T_c may no longer be visible. The calculated value of T_c ($\sim 0.3T_F$) at unitarity is in good agreement with experiment [8, 58] and other theoretical estimates [59]. To treat these trap effects one introduces the local density approximation (LDA) in which T_c is computed under the presumption that the chemical potential $\mu \rightarrow \mu - V(r)$. Here we consider a spherical trap with $V(r) = \frac{1}{2}m\omega^2 r^2$. The Fermi energy E_F is determined by the total atom number N via $E_F \equiv k_B T_F = \hbar\omega(3N)^{1/3} \equiv \hbar^2 k_F^2/2m$, where k_F is the Fermi wavevector at the center of the trap. It can be seen that the homogeneous curve is effectively multiplied by an “envelope”

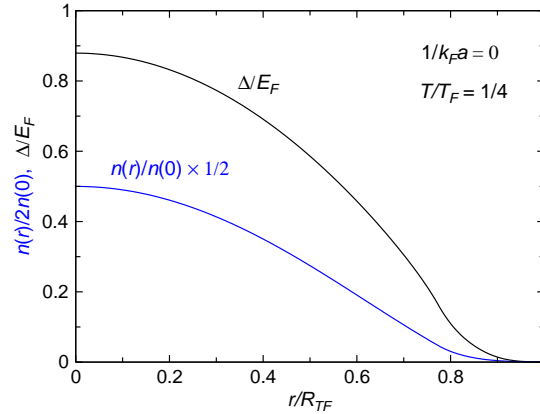


Figure 6. – Typical spatial profile for density $n(r)$ and fermionic excitation gap $\Delta(r)$ of a Fermi gas in a trap. The curves are computed at $T = T_F/4$ and at unitarity, where $1/k_F a = 0$. Here R_{TF} is the Thomas-Fermi radius, which gives the cloud size at $T = 0$ in the noninteracting limit.

curve when a trap is present. This envelope, with a higher BEC asymptote, reflects the fact that the particle density at the center of the trap is higher in the bosonic, relative to the fermionic case. In this way T_c is relatively higher in the BEC regime, as compared to its counterpart in the homogeneous case.

Figure 6 is a central one, for it prepares us for understanding various experiments. It presents a plot of the position dependent excitation gap $\Delta(r)$ and particle density $n(r)$ profile over the extent of the trap. An important point needs to be made: because the gap is largest at the center of the trap, bosonic excitations will be dominant there. At the edge of the trap, by contrast, where fermions are only weakly bound (since $\Delta(r)$ is small), the excitations will be primarily fermionic. We will see the implications of these observations as we examine thermodynamic [60] and radio frequency (RF) spectra data [61] in the ultracold gases.

One should appreciate that temperature is not straightforward to measure in these cold gases; it is most readily measured at the Fermi gas endpoint [3] or in the deep BEC regime [62]. At unitarity, the physical temperature can be extracted using phenomenological fits to the particle density profiles based on the universality hypothesis [63, 58, 64] with proper re-calibration [8, 65] below T_c . For a more general magnetic field one has to resort to adiabatic sweep thermometry [60, 66]. Here, the magnetic field of interest is accessed via a slow, adiabatic, or isentropic, magnetic field sweep starting from either the BCS or BEC endpoints, where the temperature (and the entropy [67]) are known. A finite temperature theory of BCS-BEC crossover is required to calculate the entropy [60] at general magnetic fields. In this way, the physical temperature can be associated with the measured endpoint temperature. Indeed, we will see below that the temperature which appears in the measured superfluid phase diagram [3] or in the RF pairing gap experiments [62] is given in terms of the endpoint temperature.

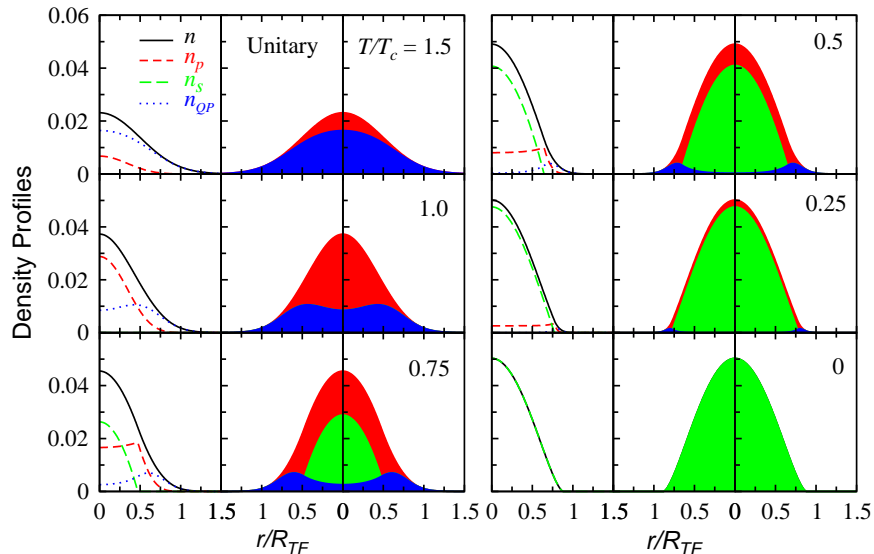


Figure 7. – Decomposition of density profiles at various temperatures at unitarity. Here green (light gray) refers to the condensate, red (dark gray) to the noncondensed pairs and blue (black) to the excited fermionic states. $T_c = 0.27T_F$, and R_{TF} is the Thomas-Fermi radius. The presence of noncondensed pairs is essential [65] for explaining why there are no sharp features in these profiles, associated with the interface of the normal and superfluid regions. Here n_s , n_p , and n_{QP} denote density of superfluid, incoherent pairs, and fermionic quasiparticle, respectively.

4. – Experimental Evidence for a Pseudogap in Cold Gases

Our finite temperature generalization of the BCS-like ground state has introduced the concept of a “pseudogap”. This pseudogap in the fermionic spectrum should be viewed as synonymous with the concept of noncondensed pairs, or with pairs which have a finite center of mass momentum. They are important both above and below T_c . In this section we want to explore the evidence for these noncondensed pairs using three different experiments: density profiles, normal state thermodynamics and RF pairing gap spectroscopy. In this section we will consider the case of an unpolarized gas.

In Fig. 7 we plot a decomposition of the particle density profiles [65] for various temperatures above and below T_c . The various color codes (or gray scales) indicate the condensate along with the noncondensed pairs and the fermions. This decomposition is based on the superfluid density so that all atoms participate in the condensation at $T = 0$.

An important observation should be noted. The noncondensed pairs are responsible for smoothing out what otherwise would be a discontinuity between the fermionic and condensate contributions. This leads to a featureless profile, in agreement with experiment [68, 69]. Indeed, these experimental observations presented a challenge for previous theories [70, 63] which ignored noncondensed pairs, and therefore predicted an effectively bimodal profile with a kink at the edge of the superfluid core. One can see from the figure that even at T_c , the system is different

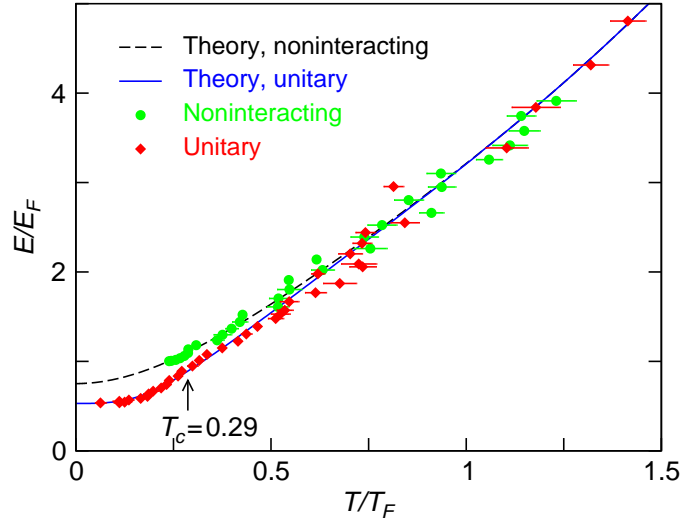


Figure 8. – Pseudogap effects as apparent from thermodynamics. From Ref. [8]. The fact that the experimental data (symbols) (and the two theoretical curves) for noninteracting and unitary Fermi gases do not merge until higher $T^* > T_c$ is consistent with the presence of a normal state pseudogap.

from a Fermi gas. That is, noncondensed pairs are present in the central region of the trap when the condensate is gone. Even at $T/T_c = 1.5$ there is a considerable fraction of noncondensed pairs. It is not until around $T^* = 2T_c$ for this unitary case, that noncondensed pairs have finally disappeared.

We next turn to a detailed comparison of theory and experiment for thermodynamics. Figure 8 presents a plot of energy E as a function of T comparing the unitary and non-interacting regimes. The solid curves are theoretical while the data points are measured in ${}^6\text{Li}$ [8]. There has been a recalibration of the experimental temperature scale in order to plot theory and experiment in the same figure. The latter was determined via Thomas-Fermi fits to the density profiles. To arrive at the calibration, we applied the same fits to the theoretically produced density profiles, examples of which appear in Fig. 7. Good agreement between theory and experiment is apparent in Fig. 8. In the figure, the temperature dependence of E reflects primarily fermionic excitations at the edge of the trap, although there is a small bosonic contribution as well. Importantly one can see the effect of a pseudogap in the unitary case. The temperature T^* is visible from the plots as that at which the non-interacting and unitary curves merge. This corresponds roughly to $T^* \approx 2T_c$.

Measurements [62] of the excitation gap Δ can be made more directly, and, in this way one can further probe the existence of a pseudogap. This pairing gap spectroscopy is based on using a third atomic level, called $|3\rangle$, which does not participate in the superfluid pairing. Under application of RF fields, one component of the Cooper pairs, called $|2\rangle$, is excited to state $|3\rangle$. If there is no gap Δ then the energy it takes to excite $|2\rangle$ to $|3\rangle$ is the atomic level splitting ω_{23} . In the presence of pairing (either above or below T_c) an extra energy Δ must be input to excite the state $|2\rangle$, as a result of the breaking of the pairs. Figure 9 shows a plot of the spectra for

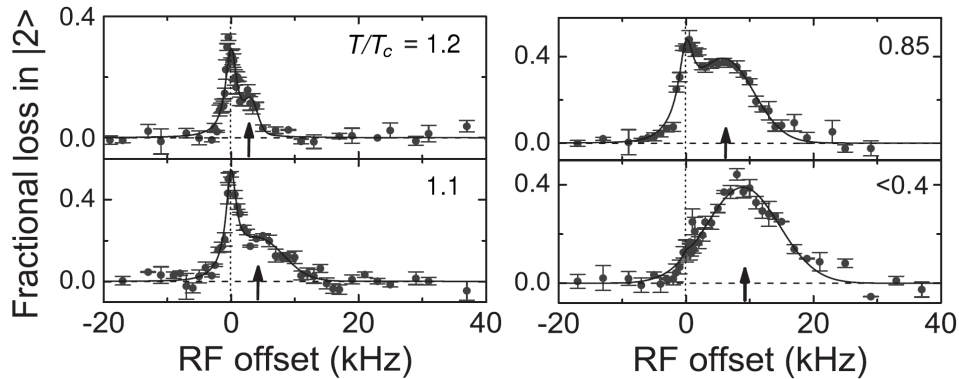


Figure 9. – Experimental RF Spectra for ${}^6\text{Li}$ at unitarity at 834 G. The temperatures labeled in the figure were computed theoretically at unitarity based on adiabatic sweeps from BEC. The two top curves, thus, correspond to the normal phase, thereby, indicating pseudogap effects. Here $E_F = 2.5\mu\text{K}$, or 52 kHz. From Ref. [62].

${}^6\text{Li}$ near unitarity for four different temperatures, which we discuss in more detail below. In general for this case, as well as for the BCS and BEC limits, there are two peak structures which appear in the data and in the theory [71, 61]: the sharp peak at $\omega_{23} \equiv 0$ which is associated with “free” fermions at the trap edge and the broader peak which reflects the presence of paired atoms; more precisely, this broad peak derives from the distribution of Δ in the trap. At high T (compared to Δ), only the sharp feature is present, whereas at low T only the broad feature remains. The sharpness of the free atom peak can be understood as coming from a large phase space contribution associated with the $2 \rightarrow 3$ excitations [61]. These data alone do not directly indicate the presence of superfluidity, but rather they provide strong evidence for pairing.

It is interesting to return to discuss the temperatures in the various panels. What is measured experimentally are temperatures T' which correspond to the temperature at the start of an adiabatic sweep from the BEC limit to unitarity. Here fits to the BEC-like profiles are used to deduce T' from the shape of the Gaussian tails in the trap. Based on knowledge [60] about thermodynamics (energy E in the previous figure or, equivalently, entropy S), and given T' , one can then compute the final temperature in the unitary regime, assuming S is constant. Indeed, this adiabaticity has been confirmed experimentally in related work [69]. We find that the four temperatures are as indicated in the figures. Importantly, one can conclude that the first two cases correspond to a normal state, albeit not far above T_c . In this way, these figures suggest that a pseudogap is present as reflected by the broad shoulder above the narrow free atom peak.

5. – Establishing Superfluidity in Cold Fermi Gases

From the time of the earliest discoveries [72, 1-8] there was a drive to establish the existence of superfluidity which is more difficult on the BCS than on the BEC side [2, 1] of the resonance. There has been a sequence of experiments which have effectively made this case, beginning first with fast sweep experiments [3, 4], then thermodynamical measurements [8], and finally

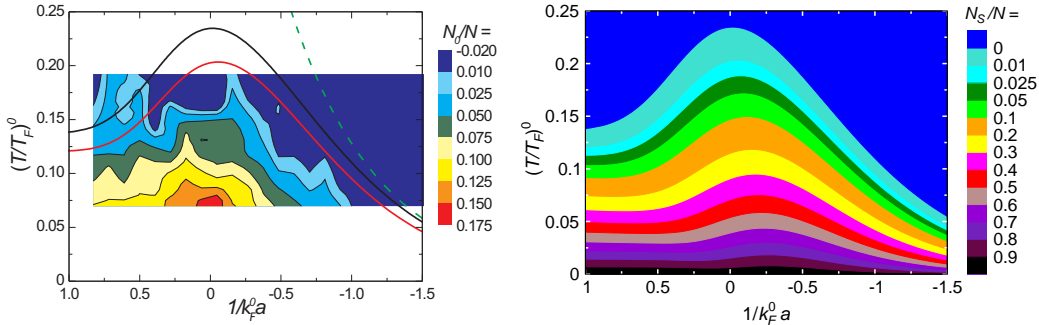


Figure 10. – (Color) Earliest evidence for superfluidity: phase diagram of ^{40}K as a function of $(T/T_F)^0$ and $1/k_F^0 a$. This compares both experiment (left panel) and theoretical computations (right panel). In the left panel, a contour plot of the measured condensate fraction N_0/N as a function of $1/k_F^0 a$ and effective temperature $(T/T_F)^0$ is compared with theoretically calculated contour lines at $N_s/N = 0$ (at the superfluid transition, black curve) and 0.01 (red curve). The experimental data have an overall systematic uncertainty of approximately 0.1 in $1/k_F^0 a$. The experimental contour at $N_0/N = 0.01$ and the theoretical line for $N_s/N = 0.01$ are in good agreement. The dashed line represents the naive BCS result $T_c/T_F^0 \approx 0.615e^{\pi/2k_F^0 a}$. The right panel represents a more complete theoretically computed equilibrium phase diagram, with contour lines for N_s/N . Here all temperatures are measured in the Fermi gas regime. From Ref. [73].

detection of quantized vortices [5]. We discuss the first two methodologies here in the context of our theoretical framework. We limit our discussion first to the case of unpolarized superfluids.

The left panel in Fig. 10 is a plot of the first phase diagram representing the condensate fraction vs $1/k_F^0 a$, as obtained in Ref. [3] for ^{40}K . Subsequently, similar studies [4] were undertaken for ^6Li . The figure is based on starting the system off in the free Fermi gas regime where it can be associated with an initial known temperature $(T/T_F)^0$, and then adiabatically sweeping closer to unitarity. [Here $T_F = T_F^0$, $k_F = k_F^0$ and $(T/T_F)^0$ are all measured in the noninteracting Fermi gas limit]. Once the near-unitary gas (of fixed entropy) is obtained, a fast sweep is made to the BEC regime, where the condensate fraction can be read off from a bi-modal profile. The presumption here, for which there is considerable experimental support [3, 4], is that, even if the condensate fraction is not conserved upon a fast sweep to BEC, the presence or absence of a condensate will be preserved. The time frame for the sweep will not allow a condensate to form in the BEC if there were none present near unitarity, nor will it allow a condensate to disappear if it was present initially.

The lines drawn on top of the experimental contour plots are the calculated [73] condensate fraction contours as a function of the adiabatic sweep-projected temperatures $(T/T_F)^0$ for 0% and 1% condensate fraction. These essentially correspond to the normal-superfluid phase boundary which is expected to be rather well measured in these sweep experiments. The figure to the right presents a full plot of the theoretical condensation fraction, importantly, measured with respect to the adiabatic sweep-projected temperatures $(T/T_F)^0$. This, then, is the theoretical phase diagram. For the 1% case, the overall trends yield good agreement between theory and

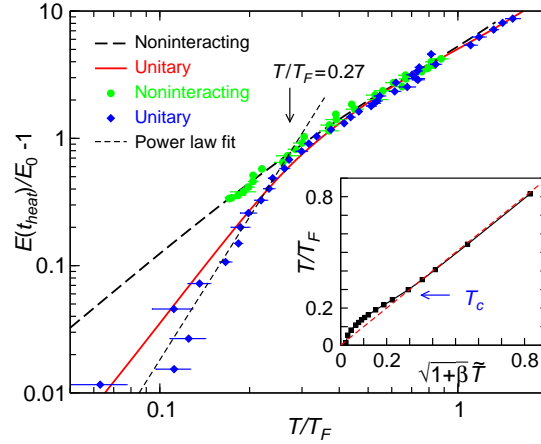


Figure 11. – Evidence for a superfluid phase via plots of the energy E vs physical temperature T . The upper curve (long dashed line) and data points correspond to the BCS or essentially free Fermi gas case, and the lower curve and data correspond to unitarity. The latter provide indications for a phase transition via a slope change. The thin dashed line represents a power law fit to the unitary data below the transition. The inset shows how temperature must be recalibrated below T_c . Here β is a parameter which characterizes the interaction energy at unitarity for $T = 0$, and \tilde{T} is an empirical temperature scale. From Ref. [8].

experiment, except for the small “overshoot” (of unknown origin) which appears in the BEC side of the data.

The second generation experiments which helped to establish superfluidity were based on thermodynamical measurements. In Fig. 11 we show data from Ref. [8]. What is plotted is the measured energy as a function of temperature on a log-log scale. This temperature represents a theoretical recalibration of an effective profile-measured temperature \tilde{T} . The key feature here is that the data (indicated by the points) show an abrupt change at a temperature one can call T_c . This abrupt change occurs for the unitary scattering case. No such feature is seen for the noninteracting Fermi gas, also plotted in the figure. Furthermore, this abrupt change in E vs T is seen *even in the raw data points* (not shown here), without appealing to a theoretical recalibration. All of this is very suggestive of a specific heat discontinuity, which is to be associated with a phase change – presumably to a superfluid phase.

The inset in the figure shows how the effective temperature \tilde{T} which is obtained from a Thomas-Fermi fit to the calculated density profile compares with the physical temperature T . The inset shows that a recalibration is necessary only below T_c , to account for the presence of a condensate. We stress that the observation of a phase change made by the Duke group [8] is not dependent on this recalibration. Hence these experiments provide good evidence for a transition between a normal and superfluid phase.

The last generation experiment to make the case for superfluidity was the observation of quantized vortices by the MIT group [5]. These very convincing experiments will be discussed elsewhere in this lecture series.

6. – Fermi Gases with Imbalanced Spin Population

The latest excitement in the field of trapped fermions pertains to gases with deliberately imbalanced spin populations [20-22]. In large part this is motivated by interest from theorists in other disciplines such as dense QCD and (isospin asymmetric) nuclear matter [11-13, 74]. From the condensed matter viewpoint there has been an underlying interest in exotic and intriguingly elusive phases associated with Zeeman effects in superconductors, such as that proposed by Larkin and Ovchinnikov and by Fulde and Ferrell (LOFF). In the LOFF state [23] the condensate has a net momentum of a fixed \mathbf{q} or of $+\mathbf{q}$ and $-\mathbf{q}$. Even more elaborate crystalline lattices of various \mathbf{q}_i have also been contemplated [24]. An additional, and very important motivation for these studies is associated with the recent claims [22] that when there is a population imbalance, the density profiles will indicate whether or not superfluidity is present and they, moreover, provide an internal mechanism for thermometry. Thus, because these experiments are claimed to identify T_c itself, and because they pertain to thermometry, it should be clear that a theoretical analysis of these experiments requires an understanding of the effects of $T \neq 0$.

We begin our discussion by summarizing some key experimental observations [20-22]. In a trapped cloud there appears to be a superfluid core, which, at the lowest temperatures, is unpolarized. Outside of this core there is a normal region, in which both spin components are present and this carries a significant fraction of the polarization. Beyond this “mixed, normal region” there is a free Fermi gas composed of the majority spin species, which carries additional polarization. At sufficiently low temperatures, there appears to be a form of phase separation in which the superfluid and normal phases are associated with zero and finite polarization, respectively.

We turn now to a theoretical understanding [56, 75] of these experiments at $T \neq 0$ first for the case of a homogeneous gas, and then later in the trapped configuration. There has been some work along these same lines elsewhere in the literature [49], although without incorporating noncondensed pair effects. We focus on the Sarma or breached pair phase [76]. The figures we present do not include the more exotic LOFF or phase separated states. The formal structure for addressing the former [55] is very similar to that of the Sarma state; we will defer a brief discussion of these until the end. To help with the clarity of the presentation, we state our major conclusions for the homogeneous and trapped configurations in the unitary regime, at the outset.

- In the *homogeneous* case temperature serves to stabilize the polarized superfluid phase. Such a phase is unstable in the ground state.
- In a *trap* at low T , the superfluid core remains unpolarized. Except at very low T , spin polarization will be mostly carried by fermions coexisting with strongly interacting, thermally excited noncondensed pairs which appear outside the core. Thus, pseudogap effects, which have been emphasized throughout, are very important here.
- With increasing T , polarization tends to continuously penetrate into the superfluid core of the trap, until at, or even below T_c , the polarization is uniformly distributed throughout the cloud.
- This superfluid Sarma or breached pair phase is limited in the amount of polarization it can accommodate, especially near unitarity. This applies to both traps and homogeneous

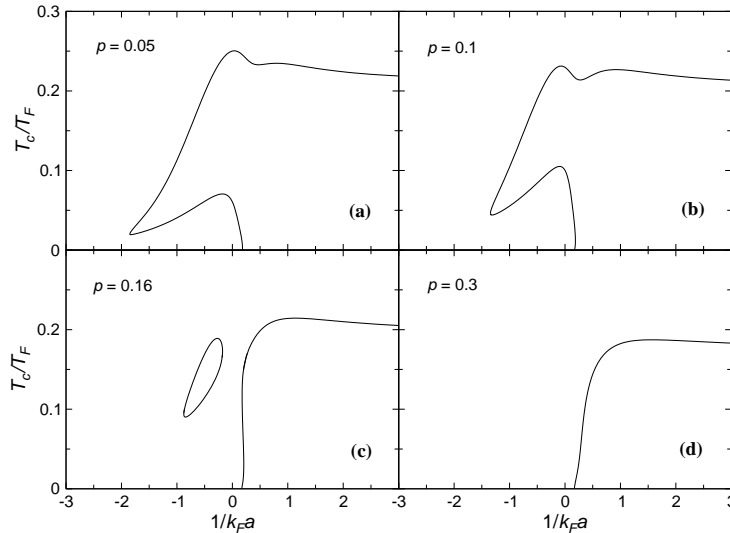


Figure 12. – Typical behavior of T_c as a function of $1/k_F a$ for spin polarizations $p = 0.05, 0.1, 0.16,$ and 0.3 . The T_c curve splits into two disconnected curves around $p = 0.14$. This figure should be compared with left panel of Fig. 5 for the unpolarized case. From Ref. [75].

systems.

Figure 12 presents a plot of T_c for a homogeneous system as a function of $1/k_F a$ for various polarizations. This figure should be compared with the left panel of Fig. 5. With this comparison, one sees at once that there can be no superfluidity in the deep BCS regime, once the polarization is different from zero. And when superfluidity first appears on the BCS side of resonance it is associated with two T_c 's at given $1/k_F a$. The larger the polarization p , the harder it is for a homogeneous system to support superfluidity, except in the BEC regime.

To understand the meaning of these two T_c 's we plot the superfluid density $n_s(T)$ as a function of T in Fig. 13, for several different values of $1/k_F a$. If one focuses on the unitary case, for definiteness, one can see that n_s vanishes at two different temperatures. The lower T_c corresponds to the onset of superfluidity. At temperatures below this, the (breached pair or Sarma) state is unstable. Similarly, at the upper T_c , superfluidity disappears in the usual way; it is destroyed by thermal excitations. For positive values of $1/k_F a$, the figure shows that the $n_s(T)$ curves stop abruptly. This is indicated by the dotted segments of the curves which represent thermodynamically unstable solutions.

The fact that T_c may be double-valued could have been anticipated in a simpler set of calculations performed at the strict mean field level, and discussed elsewhere in the literature [74]. Here one solves Eqs.(2.11) and (2.12) only, without imposing (2.20) and (2.21). In Fig. 14, we present a plot of T_c^{MF} as a function of $1/k_F a$ for a range of p . This quantity can be viewed as the pairing onset temperature T^* , when there is a stable superfluid phase. In the inset of Fig. 14 we plot $\Delta(T)$ at different $1/k_F a$ for $p = 0.3$. For $p < 0.9$ and sufficiently low T_c^{MF} , we find that

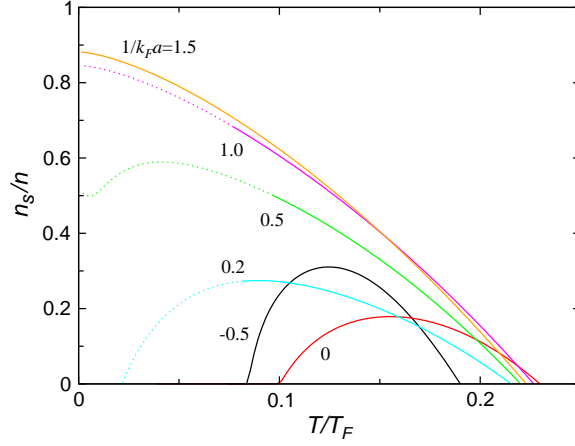


Figure 13. – Normalized superfluid density n_s/n as a function of T/T_F at $p = 0.1$ for various $1/k_F a$ from BCS to BEC. The dotted (segments of the) curves represent unstable solutions. The fact that at resonance and on the BCS-side there are two T_c' s is consistent with the previous Figure. From Ref. [75].

there are two T_c^{MF} values. This structure implies that Δ is nonmonotonic [74] in T , as indicated by the bottom curve in the inset of Fig. 14. The two zeroes of Δ represent the two values of T_c^{MF} . In contrast to the more conventional behavior (shown in the top curve for stronger pairing interaction), Δ *increases* initially with T at low temperature when $1/k_F a$ is sufficiently small.

We summarize by noting that these results indicate that *temperature enables pairing associ-*

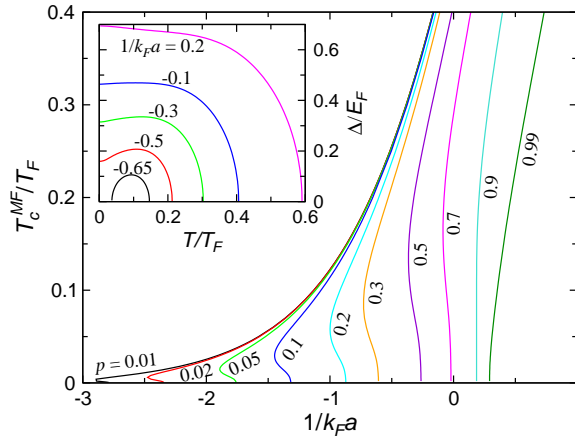


Figure 14. – Mean-field behavior of T_c^{MF} as a function of $1/k_F a$ for different spin polarizations p . Shown in the inset is the pairing gap $\Delta(T)$ at different $1/k_F a$ for $p = 0.3$ which can vanish at two distinct temperatures. Here $E_F \equiv k_B T_F \equiv \hbar^2 k_F^2 / 2m$ is the noninteracting Fermi energy in the absence of polarization. The quantity T_c^{MF} represents the pairing onset temperature T^* .

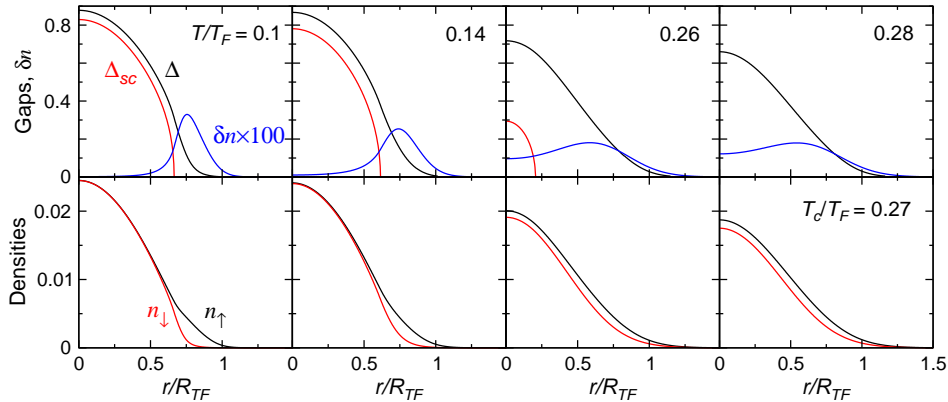


Figure 15. – Spatial profiles of the Gap (Δ), order parameter (Δ_{sc}), and the density of the up (n_{\uparrow}) and down (n_{\downarrow}) spin components and their difference (δn) for a unitary gas in a trap at $T/T_F = 0.1, 0.14, 0.26,$ and 0.28 , from left to right. Except at very low T , most of the polarization is carried by fermions co-existing with noncondensed pairs, *i.e.*, in the pseudogap regime where $\Delta_{sc} = 0$, but $\Delta \neq 0$. Here $T_c/T_F \approx 0.27$.

ated with the breached pair or Sarma state. This was also inferred in Refs. [49] and [74]. In general superfluids, one would argue that these two effects compete. We may view, then, this unusual polarized phase as an “intermediate temperature superfluid”.

We now turn to the behavior of these superfluids in a trap. The same calculations are applied to the Sarma or breached pair state using the LDA to incorporate trap effects. Figure 15 shows the resulting behavior at unitarity for polarization of 15% and for various temperatures from below to just above T_c . The upper panels plot the order parameter Δ_{sc} and the (total) gap parameter Δ . Superposed on these plots is the polarization δn . The lower panels present the density profiles for each spin state. Several important features can be gleaned from the upper panels. At the lowest temperatures the bulk of the polarization is in a region where $\Delta_{sc} = 0$, but $\Delta \neq 0$; thus polarization is excluded at low T from the superfluid core. Moreover, it can be seen that an excitation gap Δ is present throughout most of the cloud. Whenever $\Delta \neq 0$ one can infer that both spin states are present. For non-zero Δ , the particle profiles are necessarily different from those of a non-interacting gas. The bulk of the polarization appears in the “normal, mixed region”, and within this portion of the trap there are strong interactions between the two spin states. Only at the very edge of the trap is there an exclusively majority component (and here $\Delta = 0$). This region is occupied by a non-interacting Fermi gas and can thereby be used to set the temperature scale for the trapped cloud.

We end this Section with some comparisons with experiment. We address qualitative effects in Fig. 16 and semi-quantitative effects in Fig. 17. The former is for the unitary case and the latter is in the BEC regime. The left panels in Fig. 16 show data from the Rice group Ref. [77]. The upper figure plots the density profiles for each spin state and the lower panel, their difference. The unpolarized core is evident, as is the sharp edge beyond which polarization abruptly appears. This behavior has been interpreted [21, 77] as suggesting phase separation.

Because the aspect ratios for the trap are not maintained in the profiles, it has been argued

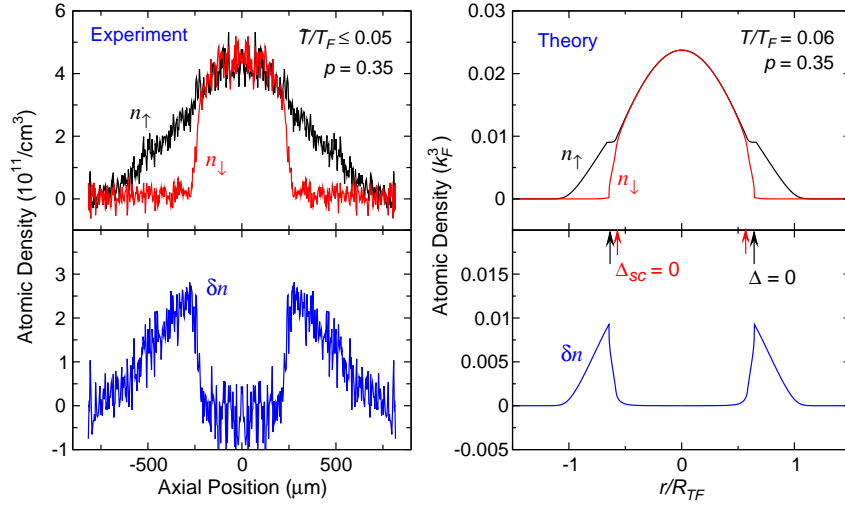


Figure 16. – Comparison of theoretically computed density distributions of the up and down spin components (upper row) and their difference (lower row) at unitarity with the Rice group data. The central issue here is not the quantitative comparison, but rather that (as seen in the theoretical curves) polarization is confined to outside the superfluid core. In the Rice data, n_{\downarrow} has a narrower distribution due to non-LDA effects. Data from Ref. [77].

[21, 77] that the LDA scheme may not be appropriate for addressing experiments on these highly anisotropic traps. In the experimental data, non-LDA effects lead to a narrower distribution for n_{\downarrow} along the axial direction while it is broadened in the radial direction. Despite this caveat we plot our counterpart theoretical results at $T = 0.06T_F$ (right panels) for qualitative comparison. This plot is designed primarily to introduce theoretical observations (which can be superposed, in effect, on the experimental plot) concerning where the superfluid phase resides in the trap. This knowledge cannot be directly gleaned from these particular experiments. These low T theoretical results are rather striking, for they make it clear that when the order parameter is present the polarization is excluded. Rather, the polarization appears in the Fermi gas region outside the condensate core. At higher T and lower p (e.g, $T = 0.1T_F$, $p = 0.15$), the polarization is carried largely within the “pseudogap” regime, where there are strong pairing correlations, but no long range order.

We turn finally to a comparison of data from the MIT group [22], and in the BEC regime. The experimental data (for polarizations near 0.6) are plotted on the two right panels which show the particle density profiles for each spin state and their difference δn . The upper panels correspond to temperatures which are believed to be in the normal state, whereas, the lower panels are for the superfluid phase. The lightly dotted curves in the experiment represent extrapolations of the Thomas-Fermi fits to the curves at large radii. In the superfluid phase, the data show that the polarization at the core center is considerably smaller than it is for the normal state. One apparent difference between above and below T_c experiments, is that at low T (i) the minority component has contracted into the center of the trap. (ii) Another signature is a kink in the majority profile.

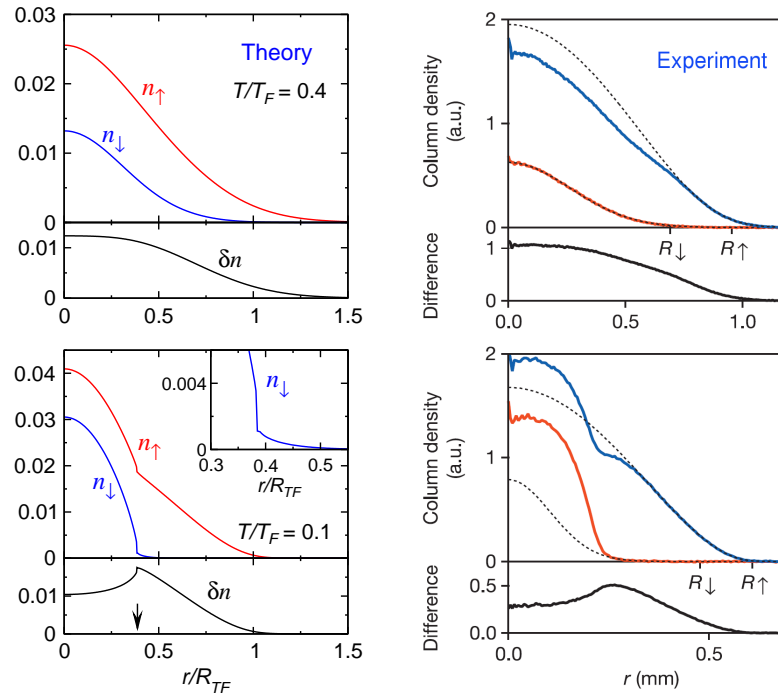


Figure 17. – Comparison of theoretically computed density distributions of the up and down spin components and their difference δn at different temperatures in the BEC regime with MIT data from Ref. [22], for $p = 0.6$. Upper/lower panels are above/below T_c . The arrow in the bottom theoretical curve for δn indicates the condensate edge which is reflected in features in both n_\uparrow and n_\downarrow , much as in the data.

Yet another signature is that (iii) there is a clear bi-modality in the minority component.

This behavior can be compared with the theoretical results plotted in the left two panels above and below T_c for a polarization $p = 0.6$. The kink in the majority component at low T can be clearly attributed to the edge of the condensate as denoted by the vertical arrow (where $\Delta_{sc} = 0$). The bi-modality in the minority component is amplified in the lower inset to make it more evident. These theoretical plots, at a qualitative level, exhibit the three central features of the data noted above.

7. – Conclusions

Throughout this Review we have stressed that temperature is important in understanding and characterizing the ultracold Fermi gases. Experimentally, one is never strictly at $T = 0$; as a result there are thermal excitations of the gas which need to be characterized both theoretically and experimentally. At a formal level, we have discussed how temperature enters into the standard BCS-BEC crossover theory by leading to a distinction between the superconducting order parameter Δ_{sc} and the gap parameter Δ . This difference reflects the existence of pre-formed

pairs above T_c and noncondensed pairs below.

At a more physical level we have shown how temperature changes the character of the gas from a superfluid at low T to an unusual (but strongly interacting) normal fluid at moderate T , and to ultimately a free Fermi gas at high T . This strongly interacting normal fluid is most interesting, for unlike the Landau Fermi liquid (or gas) which exists just above T_c in a strictly BCS superfluid, here there is a normal state excitation gap or pseudogap. By looking at three different experiments, we have provided evidence for this normal state excitation gap (in RF pairing gap spectroscopy [62] and in thermodynamics [8] and for the below- T_c counterpart (noncondensed pairs), via the shape of the particle density profiles [68, 69].

In this Review we have discussed how temperature can be measured through adiabatic sweep thermometry [3] and through Thomas-Fermi fits to density profiles [68, 8]. We have shown how temperature played an important role in establishing the first generation and earliest evidence for superfluidity – based on fast sweep experiments which yield [3] a phase diagram in the temperature vs $1/k_F a$ plane. It also played an important role in the second generation indications for superfluidity associated with thermodynamical measurements [8].

Finally, we have addressed a new and exciting class of experiments [20-22] involving spin population imbalance and shown that here too temperature plays a critical role. From an experimental point of view, the most exciting features of these experiments are that they show how the density profiles can be used to establish the transition temperature T_c . Moreover, through the wings of the profiles, they provide a theory-independent mechanism for thermometry. From our theoretical perspective, which focuses on temperature [75, 56], what is also exciting is that (i) the stability and character of these polarized superfluids is very sensitive to temperature and (ii) even in the normal state one sees strong interactions between the two spin components, which we associate with the finite T pseudogap effects we have been discussing in this Review. As stated in Ref. [22], “Already at high temperatures, above the phase transition, the larger [majority] cloud’s profile is strongly deformed in the presence of the smaller [minority] cloud, a direct signature of interaction.”

Our discussion, thus far, has not addressed phase separation [42] or the exotic LOFF states [23, 25] associated with polarized superfluids. The latter, which correspond to a condensate with a finite momentum \mathbf{q} , may well be ground states of these spin polarized gases for some range of scattering lengths a , since the polarized BCS like phase (with $\mathbf{q} = 0$) is only stable at intermediate temperatures. These LOFF phases are discussed elsewhere in this volume. There are arguments in the literature that in some more general form they play an important role near unitarity [48, 40] in trapped gases. At a theoretical level, LOFF states may be included [55] following the formalism we have outlined in this Review.

Underlying the interest in this general field of ultracold gases is the possibility that they may shed light on the high temperature cuprate superconductors either in the context [17, 19] of the BCS-BEC crossover scenario or in the context of optical lattices and Hubbard model simulations. For the former, one can return to the question of where they would fit on a phase diagram plot (such as that presented in Fig. 5 which addresses T_c vs $1/k_F a$). When the calculations are properly redone for d -wave pairing on nearly two dimensional lattices, the values and shape of the T_c curve are in quite good agreement with experiment [16-18]. Moreover, T_c vanishes well before the BEC limit is reached [26]; one can, then, deduce that in this scenario the cuprates are

close to the unitary regime, just as are the ultracold gases.

Whether or not this crossover picture turns out to be correct for high T_c , another very important rationale for its study is the possibility of generalizing what is undoubtedly the most successful theory in condensed matter physics: BCS theory. We now understand from the ultracold gases that the nature-made superconductors to which the original theory has been applied, are only a very special case of a much more general class of superfluids. And it is most fitting on this fiftieth anniversary of BCS that we pay homage to this most remarkable of theories by recognizing its even greater generality.

* * *

We wish to warmly thank all our past collaborators who have contributed to the work and figures presented here: Jelena Stajic, Yan He and Chih-Chun Chien, as well as John Thomas, Joe Kinast and Andrey Turlapov, as well as Murray Holland, Marilu Chiofalo and Josh Milstein, as well as Debbie Jin, Cindy Regal and Markus Greiner. This work was supported by NSF PHY-0555325 and NSF-MRSEC Grant No. DMR-0213745.

REFERENCES

- [1] GREINER M., REGAL C. A. and JIN D. S., *Nature (London)*, **426** (2003) 537.
- [2] JOCHIM S., BARTENSTEIN M., ALTMAYER A., HENDL G., RIEDL S., CHIN C., DENSCHLAG J. H. and GRIMM R., *Science*, **302** (2003) 2101.
- [3] REGAL C. A., GREINER M. and JIN D. S., *Phys. Rev. Lett.*, **92** (2004) 040403.
- [4] ZWIERLEIN M. W., STAN C. A., SCHUNCK C. H., RAUPACH S. M. F., KERMAN A. J. and KETTERLE W., *Phys. Rev. Lett.*, **92** (2004) 120403.
- [5] ZWIERLEIN M. W., ABO-SHAER J. R., SCHIROTZEK A. and KETTERLE W., *Nature (London)*, **435** (2005) 170404.
- [6] KINAST J., HEMMER S. L., GEHM M. E., TURLAPOV A. and THOMAS J. E., *Phys. Rev. Lett.*, **92** (2004) 150402.
- [7] BARTENSTEIN M., ALTMAYER A., RIEDL S., JOCHIM S., CHIN C., DENSCHLAG J. H. and GRIMM R., *Phys. Rev. Lett.*, **92** (2004) 203201.
- [8] KINAST J., TURLAPOV A., THOMAS J. E., CHEN Q. J., STAJIC J. and LEVIN K., *Science*, **307** (2005) 1296.
- [9] BOURDEL T., KHAYKOVICH L., CUBIZOLLES J., ZHANG J., CHEVY F., TEICHMANN M., TARRUEL L., KOKKELMANS S. J. and SALOMON C., *Phys. Rev. Lett.*, **93** (2004) 050401.
- [10] PARTRIDGE G. B., STRECKER K. E., KAMAR R. I., JACK M. W. and HULET R. G., *Phys. Rev. Lett.*, **95** (2005) 020404.
- [11] GUBANKOVA E., SCHMITT A. and WILCZEK F., *Phys. Rev. B*, **74** (2006) 064505.
- [12] LIU W. V. and WILCZEK F., *Phys. Rev. Lett.*, **90** (2003) 047002.
- [13] FORBES M. M., GUBANKOVA E., LIU W. V. and WILCZEK F., *Phys. Rev. Lett.*, **94** (2005) 017001.
- [14] LEGGETT A. J., *Diatomic molecules and Cooper pairs*, in *Modern Trends in the Theory of Condensed Matter*, ed. by PEKALSKI A. and PRZYSTAWA J., (Springer-Verlag, Berlin), 1980, pp. 13-27.
- [15] EAGLES D. M., *Phys. Rev.*, **186** (1969) 456.
- [16] CHEN Q. J., KOSZTIN I., JANKÓ B. and LEVIN K., *Phys. Rev. Lett.*, **81** (1998) 4708.
- [17] CHEN Q. J., STAJIC J., TAN S. N. and LEVIN K., *Phys. Rep.*, **412** (2005) 1.

- [18] CHEN Q. J., STAJIC J. and LEVIN K., *Low Temp. Phys.*, **32** (2006) 406; [*Fiz. Nizk. Temp.*, **32** (2006) 538].
- [19] LEGGETT A. J., *Nature Physics*, **2** (2006) 134.
- [20] ZWIERLEIN M. W., SCHIROTZEK A., SCHUNCK C. H. and KETTERLE W., *Science*, **311** (2006) 492.
- [21] PARTRIDGE G. B., LI W., KAMAR R. I., LIAO Y. A. and HULET R. G., *Science*, **311** (2006) 503.
- [22] ZWIERLEIN M. W., SCHUNCK C. H., SCHIROTZEK A. and KETTERLE W., *Nature (London)*, **442** (2006) 54.
- [23] FULDE P. and FERRELL R. A., *Phys. Rev.*, **135** (1964) A550; LARKIN A. I. and OVCHINNIKOV Y. N., *Zh. Eksp. Teor. Fiz.*, **47** (1964) 1136 [*Sov. Phys. JETP*, **20** (1965) 762].
- [24] CASALBUONI R. and NARDULLI G., *Rev. Mod. Phys.*, **76** (2004) 263.
- [25] MORA C. and COMBESCOT R., *Phys. Rev. B*, **71** (2006) 214504.
- [26] CHEN Q. J., KOSZTIN I., JANKÓ B. and LEVIN K., *Phys. Rev. B*, **59** (1999) 7083.
- [27] PIERI P. and STRINATI G. C., *Phys. Rev. B*, **71** (2005) 094520.
- [28] FRIEDBERG R. and LEE T. D., *Phys. Lett. A*, **138** (1989) 423.
- [29] DEUTSCHER G., *Nature (London)*, **397** (1999) 410.
- [30] UEMURA Y. J., *Physica C*, **282-287** (1997) 194.
- [31] RANDEIRA M., *Crossover from BCS theory to Bose-Einstein condensation*, in *Bose-Einstein Condensation*, ed. by GRIFFIN A., SNOKE D. and STRINGARI S., (Cambridge Univ. Press, Cambridge), 1995, pp. 355-92.
- [32] STAJIC J., MILSTEIN J. N., CHEN Q. J., CHIOFALO M. L., HOLLAND M. J. and LEVIN K., *Phys. Rev. A*, **69** (2004) 063610.
- [33] LEE P. A., NAGAOSA N. and WEN X. G., *Rev. Mod. Phys.*, **78** (2006) 17.
- [34] PIERI P., PISANI L. and STRINATI G. C., *Phys. Rev. Lett.*, **92** (2004) 110401.
- [35] PERALI A., PIERI P. and STRINATI G. C., *Phys. Rev. Lett.*, **93** (2004) 100404.
- [36] NOZIÈRES P. and SCHMITT-RINK S., *J. Low Temp. Phys.*, **59** (1985) 195.
- [37] CHIEN C.-C., HE Y., CHEN Q. J. and LEVIN K., *Phys. Rev. A*, **73** (2006) 041603(R).
- [38] MACHIDA M. and KOYAMA T., *Phys. Rev. Lett.*, **94** (2005) 140401.
- [39] SENSARMA R., RANDEIRA M. and HO T.-L., *Phys. Rev. Lett.*, **96** (2006) 090403.
- [40] KINNUNEN J., JENSEN L. M. and TORMA P., *Phys. Rev. Lett.*, **96** (2006) 110403.
- [41] PIERI P. and STRINATI G. C., *Phys. Rev. Lett.*, **91** (2003) 030401.
- [42] SHEEHY D. E. and RADZIHOVSKY L., *Phys. Rev. Lett.*, **96** (2006) 060401.
- [43] DE SILVA T. N. and MUELLER E. J., *Phys. Rev. A*, **73** (2006) 051602(R).
- [44] HAQUE M. and STOOF H. T. C., *Phys. Rev. A*, **74** (2006) 011602.
- [45] HE L. Y., JIN M. and ZHUANG P. F., e-print cond-mat/0606322.
- [46] PAO C. H., WU S. T. and YIP S. K., *Phys. Rev. B*, **73** (2006) 132506.
- [47] PIERI P. and STRINATI G. C., *Phys. Rev. Lett.*, **96** (2006) 150404.
- [48] MACHIDA K., MIZUSHIMA T. and ICHIOKA M., *Phys. Rev. Lett.*, **97** (2006) 120407.
- [49] YI W. and DUAN L. M., *Phys. Rev. A*, **73** (2006) 031604(R).
- [50] GUBBELS K. B., ROMANS M. W. J. and STOOF H. T. C., e-print cond-mat/0606330.
- [51] CHEN Q. J., *Generalization of BCS theory to short coherence length superconductors: A BCS–Bose-Einstein crossover scenario*, Ph.D dissertation, University of Chicago, 2000.
- [52] STAJIC J., CHEN Q. J. and LEVIN K., *Phys. Rev. A*, **71** (2005) 033601.
- [53] FETTER A. L. and WALECKA J. D., *Quantum Theory of Many-Particle Systems*, (McGraw-Hill, San Francisco), 1971.
- [54] MALY J., JANKÓ B. and LEVIN K., *Physica C*, **321** (1999) 113.
- [55] CHEN Q. J., YAN H., CHIEN C.-C. and LEVIN K., preprint, cond-mat/0608662.
- [56] CHIEN C.-C., CHEN Q. J., HE Y. and LEVIN K., *Phys. Rev. A*, **74** (2006) 021602(R).
- [57] KOSZTIN I., CHEN Q. J., KAO Y. J. and LEVIN K., *Phys. Rev. B*, **61** (2000) 11662.
- [58] KINAST J., TURLAPOV A. and THOMAS J. E., *Phys. Rev. Lett.*, **94** (2005) 170404.

- [59] PERALI A., PIERI P., PISANI L. and STRINATI G. C., *Phys. Rev. Lett.*, **92** (2004) 220404.
- [60] CHEN Q. J., STAJIC J. and LEVIN K., *Phys. Rev. Lett.*, **95** (2005) 260405.
- [61] HE Y., CHEN Q. J. and LEVIN K., *Phys. Rev. A*, **72** (2005) 011602(R).
- [62] CHIN C., BARTENSTEIN M., ALTMAYER A., RIEDL S., JOCHIM S., HECKER-DENSCHLAG J. and GRIMM R., *Science*, **305** (2004) 1128.
- [63] HO T.-L., *Phys. Rev. Lett.*, **92** (2004) 090402.
- [64] THOMAS J. E., KINAST J. and TURLAPOV A., *Phys. Rev. Lett.*, **95** (2005) 120402.
- [65] STAJIC J., CHEN Q. J. and LEVIN K., *Phys. Rev. Lett.*, **94** (2005) 060401.
- [66] WILLIAMS J. E., NYGAARD N. and CLARK C. W., *New J. Phys.*, **6** (2004) 123.
- [67] CARR L. D., SHLYAPNIKOV G. V. and CASTIN Y., *Phys. Rev. Lett.*, **92** (2004) 150404.
- [68] O'HARA K. M., HEMMER S. L., GEHM M. E., GRANADE S. R. and THOMAS J. E., *Science*, **298** (2002) 2179.
- [69] BARTENSTEIN M., ALTMAYER A., RIEDL S., JOCHIM S., CHIN C., DENSCHLAG J. H. and GRIMM R., *Phys. Rev. Lett.*, **92** (2004) 120401.
- [70] CHIOFALO M. L., KOKKELMANS S. J. J. M. F., MILSTEIN J. N. and HOLLAND M. J., *Phys. Rev. Lett.*, **88** (2002) 090402.
- [71] KINNUNEN J., RODRIGUEZ M. and TÖRMÄ P., *Science*, **305** (2004) 1131.
- [72] KINAST J., TURLAPOV A. and THOMAS J. E., *Phys. Rev. A*, **70** (2004) 051401(R).
- [73] CHEN Q. J., REGAL C. A., GREINER M., JIN D. S. and LEVIN K., *Phys. Rev. A*, **73** (2006) 041601(R).
- [74] SEDRAKIAN A. and LOMBARDO U., *Phys. Rev. Lett.*, **84** (2000) 602.
- [75] CHIEN C.-C., CHEN Q. J., HE Y. and LEVIN K., *Phys. Rev. Lett.*, **97** (2006) 090402.
- [76] SARMA G., *J. Phys. Chem. Solids*, **24** (1963) 1029.
- [77] PARTRIDGE G. B., LI W. H., LIAO Y. A., HULET R. G., HAQUE M. and STOOF H. T. C., e-print cond-mat/0608455.